

1995/20944

N95-27365

SINGLE-DROP REACTIVE EXTRACTION/EXTRACTIVE REACTION WITH FORCED  
CONVECTIVE DIFFUSION AND INTERPHASE MASS TRANSFERLeonid S. Kleinman and X.B. Reed, Jr.  
University of Missouri-Rolla  
Rolla, Missouri404948  
52034  
45113  
p. 26

## SUMMARY

An algorithm has been developed for time-dependent forced convective diffusion-reaction having convection by a recirculating flow field within the drop that is hydrodynamically coupled at the interface with a convective external flow field that at infinity becomes a uniform free-streaming flow. The concentration field inside the droplet is likewise coupled with that outside by boundary conditions at the interface. A chemical reaction can take place either inside or outside the droplet, or reactions can take place in both phases.

The algorithm has been implemented, and for comparison results are shown here for the case of no reaction in either phase and for the case of an external first order reaction, both for unsteady behaviour. For pure interphase mass transfer, concentration isocontours, local and average Sherwood numbers, and average droplet concentrations have been obtained as a function of the physical properties and external flow field. For mass transfer enhanced by an external reaction, in addition to the above forms of results, we present the enhancement factor, with the results now also depending upon the (dimensionless) rate of reaction.

## INTRODUCTION

There are many industrial and environmental processes in which two-phase fluid-liquid systems are in use. Gases may be dispersed as bubbles in liquid phases, such as occurs in bubble columns and sparged vessels. Liquids may be dispersed in gases, such as occurs in scrubbers and in the atmosphere. And a liquid that is immiscible or partially miscible in another liquid may be dispersed in a liquid-liquid spray column extractor or reactor. The design of such systems may involve heat transfer, either intentionally or incidentally, but the widest range of applications involves mass transfer.

Interphase mass transfer may proceed into or out of the dispersed phase. One (or more) chemical reaction(s) may take place in either the dispersed or the continuous phase in order to enhance the rate of mass transfer. In two-phase reactions, certain of the reactants may be transferred from one phase into the other, where the reaction takes place, and the reaction products may then be transferred back into the first phase. Reactions may also occur in both phases.

Because of the finite, generally small volume of each drop or bubble, interphase mass transfer unaccompanied by chemical reaction is inherently unsteady, regardless of the direction of mass transfer. Even if there is a reaction that admits of a steady state in the drop or bubble, unsteady behavior may nevertheless be of practical even primary importance.

The continuous phase is inevitably in motion relative to the dispersed phase, and for clean systems (containing for instance no surface active agents) the motion in the two phases will be hydrodynamically coupled.

The general formulation could take into account either linear or nonlinear chemical reactions in either or both phases, and it could incorporate any velocity field that can be expressed as a function of  $r$  and  $\vartheta$ . Neither are variable properties excluded.

In order to demonstrate the utility of the algorithm, for concreteness we undertake the mathematical description of a liquid-liquid system in which a first order reaction takes place in the continuous phase. The dispersed phase is sufficiently dilute that the droplets which sediment (either falling under their weight or rising because of buoyancy) may be assumed isolated in an infinite medium, both with regard to fluid mechanics and to diffusion and reaction. The droplets are taken small enough that interfacial tension dominates shape effects and they are spherical. Although the approach we take and the methods we use do not require that that viscosity dominates flow effects and that the velocity fields have low Reynolds numbers, we nonetheless consider the hydrodynamically coupled Hadamard - Rybczinsky profile for circulation within the droplet driven by an external velocity field that becomes a uniform streaming flow far from the droplet. Physical and chemical properties are assumed constant, which would be the case for dilute isothermal systems, and we thus analyze interphase mass transfer for the forced convective diffusion-reaction single-drop system. We investigate specifically the role of the reaction rate, as measured by an appropriate Damköhler number, the solubility of the solute in the phases, as expressed by the linear distribution coefficient (Henry's law), the ratio of convection to diffusion, as measured by the Peclet number, and the ratio of the viscosities and that of molecular diffusivities of the two phases.

### GOVERNING EQUATIONS

The dimensionless forced convective diffusion-reaction equations governing the solute concentrations in the drop ( $0 \leq r \leq 1$ ) and the continuous ( $1 \leq r < \infty$ ) phases,  $i = 1, 2$ , respectively, can be represented in the form

$$\frac{\partial c^{(i)}}{\partial t} + K_c^{(i)} \mathbf{v}^{(i)} \cdot \nabla c^{(i)} = K_d^{(i)} \nabla^2 c^{(i)} - K_r^{(i)} c^{(i)}, \quad (1)$$

where  $i = 1$  corresponds to the internal domain  $0 \leq r \leq 1$ , and  $i = 2$  to the external one  $1 \leq r < \infty$ .

The dimensional parabolic partial differential equations have been rendered dimensionless using the droplet radius  $R$  as the characteristic length scale. The concentrations are measured in units of the initial driving force,

$$c^{(i)} = \frac{H^{(i)} \bar{c}^{(i)} - H \bar{c}_\infty}{\bar{c}_0 - H \bar{c}_\infty}, \quad i = 1, 2, \quad (2)$$

in which

$$H^{(i)} = \begin{cases} 1, & i = 1 \\ H, & i = 2, \end{cases} \quad (3)$$

with  $H$  the Henry's "law" distribution coefficient, and

$$t = 0: \quad \bar{c}^{(1)} = \bar{c}_0, \quad \bar{c}^{(2)} = \bar{c}_\infty. \quad (4)$$

The characteristic time scale can be selected, for example, on the basis of the fastest physical or chemical process, occurring in the system, *viz.*,

$$\tau_* = \min(\tau_{\text{conv}}^{(i)}, \tau_{\text{diff}}^{(i)}, \tau_{\text{rxn}}^{(i)}, \quad i = 1, 2), \quad (5)$$

in which

$$\tau_{\text{conv}}^{(i)} = \frac{R}{f^{(i)}(\mu) U_\infty}, \quad \tau_{\text{diff}}^{(i)} = \frac{R^2}{D^{(i)}}, \quad \tau_{\text{rxn}}^{(i)} = \frac{1}{k^{(i)}}, \quad i = 1, 2. \quad (6)$$

The diffusivities and rate constants for the first order chemical reactions are denoted by  $D^{(i)}$  and  $k^{(i)}$ , respectively, and the  $K$ 's represent different combinations of standard dimensionless parameters for different choices of  $\tau_*$ , as indicated in Table 1.

Although our numerical implementation of the algorithm requires only that the velocity fields in the two phases be separable, we have selected the Hadamard - Rybczinsky solution for the convecting velocities in the dispersed and continuous phases to establish connections with earlier research [7, 8, 9]. In this instance, the characteristic velocity in each phase, with  $U_\infty$  the freestreaming uniform flow at infinity, is taken as

$$U_*^{(i)} = f^{(i)}(\mu) U_\infty, \quad i = 1, 2, \quad (7)$$

in which

$$f^{(1)}(\mu) = \frac{1}{2(1+\mu)}, \quad f^{(2)}(\mu) = 1, \quad (8)$$

with the viscosity ratio

$$\mu = \mu^{(1)}/\mu^{(2)}. \quad (9)$$

The equations (10) are the ones used in the sequel, reflecting the selection of  $\tau_{\text{diff}}^{(2)}$  as the unit of time:

$$\begin{aligned} & \frac{\partial c^{(i)}}{\partial \tau} + \frac{Pe^{(2)}}{2} \cdot \left( v_r^{(i)} \frac{\partial c^{(i)}}{\partial r} - \frac{v_\lambda^{(i)}}{r} \sqrt{1-\lambda^2} \frac{\partial c^{(i)}}{\partial \lambda} \right) \\ &= \frac{D^{(i)}}{D^{(2)}} \cdot \left\{ \frac{1}{r^2} \frac{\partial}{\partial r} \left( r^2 \frac{\partial c^{(i)}}{\partial r} \right) + \frac{1}{r^2} \frac{\partial}{\partial \lambda} \left[ (1-\lambda^2) \frac{\partial c^{(i)}}{\partial \lambda} \right] \right\} \\ & - Da_{II}^{(i)} \frac{D^{(i)}}{D^{(2)}} \cdot \left( c^{(i)} + \frac{H \bar{c}_\infty}{\bar{c}_0 - H \bar{c}_\infty} \right), \quad i = 1, 2, \end{aligned} \quad (10)$$

with  $\lambda = \cos \vartheta$ , subject to the boundary conditions at the droplet interface,

$$r = 1: \quad \begin{cases} c^{(1)} = c^{(2)} \\ H \cdot D \frac{\partial c^{(1)}}{\partial r} = \frac{\partial c^{(2)}}{\partial r} \end{cases} \quad (11)$$

and at the limits of the overall domain,

$$r = 0: \quad c^{(1)} < \infty \quad (12)$$

$$r \rightarrow \infty: \quad c^{(2)} \rightarrow 0 \quad (13)$$

Periodic boundary conditions in the angle variable,

$$\left. \frac{\partial c^{(i)}}{\partial \vartheta} \right|_{\vartheta=0, \pi} = 0, \quad i = 1, 2, \quad (14)$$

are satisfied automatically after introduction of the new independent variable  $\lambda$ .

The concentrations are subject to the initial conditions:

$$t = 0: \quad c^{(1)} = 1, \quad c^{(2)} = 0 \quad (15)$$

The actual direction of mass transfer may be out of or into the drop, depending upon the driving force  $(\tilde{c}_0 - H\tilde{c}_\infty)$ , even though the formulation of the problem suggests transfer from the droplet.

The opposite direction of mass transfer in the actual problem would lead to the appearance of the inhomogeneous part in the reaction terms in (10) (but only when the corresponding  $K_r^{(i)} \neq 0$ ).

### THE ALGORITHM

The problem is linear, and we use the Galerkin spectral method for the spatial discretization. The advantages of this method are well known [1, 2].

Boundary conditions at the origin of the droplet (12) and at infinity (13) and the symmetry boundary conditions (15) are implemented by the Lanczos tau-method [1, 2, 14].

We express the unknown functions  $c^{(i)}(\tau, \lambda, r)$  in a customary manner,

$$c^{(i)}(\tau, \lambda, r) = \sum_{m=0}^M c_m^{(i)}(\tau, r) P_m(\lambda), \quad i = 1, 2, \quad (16)$$

in which the  $P_m(\lambda)$  are the Legendre polynomials of order  $m$  and the unknown coefficient functions  $c_m^{(i)}(\tau, r)$  are termed "radial functions" for brevity in the sequel.

The discretization in the radial direction is performed in somewhat different ways for the internal and external domains.

Using equation (10) for mass transfer inside the droplet ( $i = 1$ ), it is a simple matter to show that functions  $c_m^{(1)}(\tau, r)$  obey the following restrictions:

$$c_l^{(1)}(\tau, r = 0) = 0, \quad l \neq 0, \quad (17)$$

$$\left. \frac{\partial c_l^{(1)}}{\partial r} \right|_{r=0} = 0, \quad l \neq 1, \quad (18)$$

$$\left. \begin{array}{l} c_{2k}^{(1)}(\tau, r) - \text{even function of } r \\ c_{2k+1}^{(1)}(\tau, r) - \text{odd function of } r \end{array} \right\} k = 0, 1, \dots \quad (19)$$

On the basis of these restrictions, the radial functions inside the droplet were approximated by a series in even Chebyshev polynomials:

$$c_m^{(1)}(\tau, r) = \delta_{m,0} \cdot \alpha_0(\tau) + r^{\kappa_m} \cdot \sum_{n=1}^{N^{(1)}} \phi_{m,n}^{(1)}(\tau) T_{2n-2}(r), \quad m = 0, 1, \dots, M, \quad (20)$$

in which the  $T_p(r)$  are Chebyshev polynomials of the first kind of order  $p$ , and

$$\kappa_{2j} = 2, \quad j = 0, 1, \dots \quad (21)$$

$$\kappa_1 = 1, \quad \kappa_{2j+1} = 3, \quad j = 1, 2, \dots \quad (22)$$

Using (20) we automatically satisfy boundary condition (12) and avoid the singularity at the origin of the drop; the function  $\alpha_0(\tau)$  represents the value of the concentration at the origin.

Such an expansion on the interval  $0 \leq \tau \leq 1$  is valid as the even Chebyshev polynomials form a complete set for the type of functions considered [10].

The use of half the commonly used interval  $[-1, 1]$  permits us to double the highest order of the polynomials used, leaving the number of terms in the series unaltered.

The nonuniformity of the distribution of nodes in the spectral method (their number in close proximity to the surface is higher than near the origin) matches the physics of the problem as the concentration gradient near the interface is much larger.

For the semi-infinite external domain we implement the widely used procedure of truncating it at an appropriately large radius  $\tau_\infty$ , far enough from the interface to make negligible the disturbance introduced by truncation. The boundary condition at infinity (13) is now imposed on this artificial boundary. It could be imposed as "hard", "soft" [12] or "behavioral" [1, 13]. We use the "hard" one,

$$\tau = \tau_\infty : \quad c^{(2)} = 0 \quad (23)$$

because it immediately results in the original boundary condition (13) if  $\tau_\infty \rightarrow \infty$ .

It is necessary to realize that by doing this we are changing the physical sense of the problem. The decrease to zero of the concentration infinitely far from its source is caused physically by the spreading of a finite amount of the species over an infinite spatial volume. After introduction of the boundary sphere at  $\tau = \tau_\infty$ , we model this decrease by imposing what amounts to an infinitely fast heterogeneous reaction on the artificial boundary  $\tau_\infty$ . The only justification for this is an *a posteriori* one, viz., by checking that the increase of  $\tau_\infty$  does not alter the solution in the vicinity of the droplet and in particular the interphase mass transfer.

Our computations have confirmed this and show that when  $\tau_\infty$  is chosen sufficiently large the choice of the particular type of boundary conditions mentioned above does not influence the resultant concentration distribution in regions where its value differs significantly from zero.

The domain  $1 \leq \tau \leq \tau_\infty$  is mapped onto the interval  $-1 \leq z \leq 1$  in such a way that the point  $z = 1$  matches  $\tau = 1$  and the point  $z = -1$  matches  $\tau = \tau_\infty$ . Among the wide variety of possible mappings two are used more often than others, the exponential and rational ones [1, 2]. A comparison by Grosch and Orszag [11] has shown that the latter mapping has some advantages over the former.

Specifically, we use

$$z = \frac{\tau - (1 + \delta)}{(1 - \tau) \left(1 - \frac{2\delta}{\tau_\infty - 1}\right) - \delta}, \quad (24)$$

where  $\delta$  is the parameter representing the distance between the droplet surface and point mapped into  $z = 0$ . It is worth mentioning that we have also implemented the exponential mapping and could find no advantages for it over the rational mapping.

The radial functions in the external domain are expanded as

$$c_m^{(2)}(\tau, z) = \sum_{n=1}^{N^{(2)}} \phi_{m,n}^{(2)}(\tau) Z_n(z), \quad m = 0, 1, \dots, M, \quad (25)$$

where the  $Z_n(z)$ ,  $n = 1, 2, \dots, N^{(2)}$  are linear combinations of Chebyshev polynomials, each satisfying the boundary condition following from (13):

$$Z_n(z = -1) = 0, \quad n = 1, 2, \dots, N^{(2)}. \quad (26)$$

We take

$$Z_{2k}(z) = T_{2k}(z) - 1 \quad (27)$$

$$Z_{2k-1}(z) = T_{2k-1}(z) + 1$$

Thus, we reduce the system of partial differential equations for two initially unknown functions  $c^{(1)}(\tau, \lambda, \tau)$  and  $c^{(2)}(\tau, \lambda, \tau)$  to a larger system of ordinary differential equations in  $\tau$ , for

$$\begin{aligned} \alpha_0(\tau), \phi_{m,n_1}^{(1)}, \phi_{m,n_2}^{(2)}, \quad m = 0, 1, \dots, M, \\ n_1 = 1, 2, \dots, N^{(1)}, \quad n_2 = 1, 2, \dots, N^{(2)}. \end{aligned} \quad (28)$$

The total number of these unknown functions is  $1 + (M + 1)(N^{(1)} + N^{(2)})$ .

In order to obtain equations for these functions we use the conventional Petrov - Galerkin method, i.e., the basis functions are taken as the test functions [2]. We define two inner products:

$$(f, g)^{(1)} \equiv \int_{-1}^1 d\lambda \int_0^1 f \cdot g \frac{dr}{\sqrt{1-r^2}}, \quad (29)$$

$$(f, g)^{(2)} \equiv \int_{-1}^1 d\lambda \int_{-1}^1 f \cdot g \frac{dz}{\sqrt{1-z^2}}. \quad (30)$$

Forming by (29) the inner product of (10) for  $i = 1$  with the test functions

$$P_0(\lambda) T_0(\tau), \quad P_m(\lambda) r^m \cdot T_{2n_1-2}(\tau), \quad m = 0, 1, \dots, M, \quad n_1 = 1, 2, \dots, N^{(1)} - 1, \quad (31)$$

and by (30) the inner product of (10) for  $i = 2$  with the test functions

$$P_m(\lambda) Z_{n_2}(z), \quad m = 0, 1, \dots, M, \quad n_2 = 1, 2, \dots, N^{(2)} - 1, \quad (32)$$

we obtain two vector equations

$$\mathbf{A}^{(i)} \frac{d\phi^{(i)}}{d\tau} = (-K_c^{(i)} \mathbf{B}^{(i,c)} + K_d^{(i)} \mathbf{B}^{(i,d)} - K_r^{(i)} \mathbf{B}^{(i,r)}) \cdot \phi^{(i)} + K_r^{(i)} \mathbf{b}^{(i)}, \quad i = 1, 2. \quad (33)$$

Here  $\mathbf{A}^{(i)}$ ,  $\mathbf{B}^{(i,c)}$ ,  $\mathbf{B}^{(i,d)}$ ,  $\mathbf{B}^{(i,r)}$  are  $\{1 + (M + 1)(N^{(i)} - 1), 1 + (M + 1)N^{(i)}\}$  matrices,  $\mathbf{b}^{(i)} - \{1 + (M + 1)N^{(i)}\}$  are the vectors of inhomogeneous terms, and  $\phi^{(i)}(\tau) - \{1 + (M + 1)N^{(i)}\}$  are the unknown vectors,

$$\phi^{(1)}(\tau) = (\alpha_0, \phi_{0,1}^{(1)}, \dots, \phi_{0,N^{(1)}}^{(1)}, \dots, \phi_{M,1}^{(1)}, \dots, \phi_{M,N^{(1)}}^{(1)})^T, \quad (34)$$

$$\phi^{(2)}(\tau) = (\phi_{0,1}^{(2)}, \dots, \phi_{0,N^{(2)}}^{(2)}, \dots, \phi_{M,1}^{(2)}, \dots, \phi_{M,N^{(2)}}^{(2)})^T. \quad (35)$$

The remaining  $2(M+1)$  equations are derived from the boundary conditions (11).

Upon substituting (20) and (25) into (11), multiplying by  $P_m(\lambda)$ ,  $m = 0, 1, \dots, M$  and integrating  $\lambda$  from  $-1$  to  $1$ , we obtain two sets of  $M+1$  linear algebraic equations:

$$\mathbf{Q}^{(1)} \cdot \phi^{(1)} = \mathbf{Q}^{(2)} \cdot \phi^{(2)}, \quad (36)$$

$$\mathbf{H} \cdot \mathbf{D} \cdot \mathbf{S}^{(1)} \cdot \phi^{(1)} = \mathbf{S}^{(2)} \cdot \phi^{(2)}, \quad (37)$$

where  $\mathbf{Q}^{(i)}$ ,  $\mathbf{S}^{(i)}$  are  $\{(M+1), (M+1)(1+N^{(i)})\}$  matrices,  $i = 1, 2$ .

By expressing  $\phi_{m,N^{(1)}}^{(1)}$  and  $\phi_{m,N^{(2)}}^{(2)}$ ,  $m = 0, 1, \dots, M$ , using the system (36)–(37) and substituting in the system (33), we arrive finally at the system of  $1 + (M+1)(N^{(1)} + N^{(2)} - 2)$  linear ODEs:

$$\mathbf{A} \frac{d\phi}{d\tau} = (\mathbf{B}^{(c)} + \mathbf{B}^{(d)} + \mathbf{B}^{(r)}) \cdot \phi + \mathbf{b}. \quad (38)$$

The constant matrices  $\mathbf{B}^{(c)}$ ,  $\mathbf{B}^{(d)}$  and  $\mathbf{B}^{(r)}$  correspond respectively to the convective, diffusive, and reactive terms in the original equation (10),  $\mathbf{b}$  is an  $\{1 + (M+1)(N^{(1)} + N^{(2)} - 2)\}$  constant vector, and  $\phi(\tau)$  is the vector of unknown functions

$$\phi \equiv (\alpha_0, \phi_{0,1}^{(1)}, \dots, \phi_{0,N^{(1)}-1}^{(1)}, \phi_{0,1}^{(2)}, \dots, \phi_{0,N^{(2)}-1}^{(2)}, \dots, \phi_{M,1}^{(1)}, \dots, \phi_{M,N^{(1)}-1}^{(1)}, \phi_{M,1}^{(2)}, \dots, \phi_{M,N^{(2)}-1}^{(2)})^T \quad (39)$$

and not simply a concatenation of vectors  $\phi^{(1)}$  and  $\phi^{(2)}$ .

The matrices  $\mathbf{A}$ ,  $\mathbf{B}^{(d)}$  and  $\mathbf{B}^{(r)}$  are block-diagonal. They all have  $M+1$  nonzero square  $\{N^{(1)}+N^{(2)}-2, N^{(1)}+N^{(2)}-2\}$  matrices on their main diagonals and their first  $1+(N^{(1)}+N^{(2)}-2)$  elements in the first row and the first column are nonzero.

The matrices  $\mathbf{B}^{(c)}$  that result from transforming the convective terms also have block structure with the same block sizes. However, they are no longer block-diagonal and the amount of nonzero block-diagonals depends on the velocity fields  $v^{(i)}$ ,  $i = 1, 2$ . The higher the degree of  $\lambda$  that is involved in the velocity field expressions, the greater will be the coupling between the radial functions of different orders. And the increase of the order of this coupling leads to a corresponding increase in the number of nonzero block diagonals in  $\mathbf{B}^{(c)}$ .

For the Hadamard – Rybczinsky field, for example, these matrices are block-tridiagonal, but for the velocity field in [15], valid for higher Reynolds numbers, it would be block-pentadiagonal.

The discontinuous initial conditions (15) are not appropriate for computations. Instead, we used the analytical solution for the pure diffusion case (no convection, no chemical reaction) derived in [16]. The concentration distributions for very small time values were expanded over our basis functions  $T_{2n-2}(\tau)$  and  $Z_n$ ,  $n = 1, 2, \dots$  to initialize the computations, and the coefficients obtained were used as initial conditions for  $\alpha_0(\tau)$ ,  $\phi_{m,n_1}^{(1)}$ , and  $\phi_{m,n_2}^{(2)}$ ,  $m = 0, 1, \dots, M$ ,  $n_1 = 1, 2, \dots, N^{(1)} - 1$ ,  $n_2 = 1, 2, \dots, N^{(2)} - 1$ .

For time discretization of the system (38) we used the first-order backward Euler method. Defining  $\phi^n$  as vector  $\phi$  at the  $n$ -th time step of magnitude  $\Delta\tau$  and

$$\mathbf{B} = \mathbf{B}^{(c)} + \mathbf{B}^{(d)} + \mathbf{B}^{(r)}, \quad (40)$$

system (38) can be rewritten as

$$(\mathbf{A} - \Delta\tau\mathbf{B}) \cdot \Delta\phi^{n+1} = \Delta\tau\mathbf{B} \cdot \phi^n + \Delta\tau\mathbf{b}, \quad (41)$$

where

$$\Delta\phi^{n+1} = \phi^{n+1} - \phi^n. \quad (42)$$

Every time step system of linear equations (41) was solved by regular Gauss elimination (preceded by LU decomposition) with the following iterative refinement [3]. The matrix on the left side of (41) has the same structure as the matrix  $\mathbf{B}$ ; as mentioned, it is block-tridiagonal for the Hadamard-Rybczinsky velocity field. Our attempts to apply block-elimination methods (in particular, the block Thomas algorithm [4]) failed, presumably because block LU factorization does not involve pivoting, which is essential when diagonal dominance does not occur (which is the case for high Peclet numbers).

We considered the matrix on the left side of (41) as a banded one with bandwidth  $1 + 3(N^{(1)} + N^{(2)} - 2)$ .

As long as this matrix depends on the time step and its factorization is a time-consuming process, only two values of the time step were used for each run. A smaller one was used for an initial time period and another one for the subsequent time range.

The numbers of terms in series (16), (20), and (25) depend on the steepness of the concentration gradients and were different for different values of Peclet and Damköhler numbers. The maximum numbers used were  $M = 87$ ,  $N^{(1)} = 25$ ,  $N^{(2)} = 97$ .

As is well known [1, 2], an increase in the number of terms in a spectral series (especially in the series in Chebyshev polynomials) leads to very high condition numbers for the resulting system of linear equations. This was alleviated by using double precision in all computations and, as mentioned above by application of the iterative refinement to the solution obtained with the Gauss elimination procedure.

## QUANTITIES OF INTEREST

The most practically interesting quantity in extraction problems is the amount of material extracted by a particular instant in time. For the problem under consideration (i.e., when species are extracted from the droplet) this can be conveniently characterized by the time-dependent average dimensionless concentration of species remaining in the drop:

$$\bar{c}^{(1)} = \frac{3}{2} \cdot \int_0^1 \int_{-1}^1 r^2 c^{(1)}(\tau, \lambda, r) d\lambda dr \quad (43)$$

This quantity changes in time as a result of mass transfer out of the droplet. The local and surface average rates of this transfer are characterized by corresponding mass transfer coefficients, the quantities which when multiplied by the driving force give the respective mass transfer rate. The nondimensional mass transfer coefficient is usually referred to as the Sherwood number  $Sh$ , which is analogous to the Nusselt number in heat transfer problems.

Different kinds of Sherwood number can be introduced, depending on the driving force on which they are based and the domain to which they are related.

For the problem of single-drop extraction, the instantaneous driving force  $F^{(dx)}$  for mass transfer is the difference between the concentration of the transferring species in the droplet and that far away from it, taking into account the step change of the concentration at the interface due to solubility,

$$F^{(dr)} = \bar{c}^{(1)} - H\bar{c}_\infty, \quad (44)$$

where  $\bar{c}^{(1)}$  is the dimensional average concentration of species in the droplet.

Often the Sherwood number is based on the maximum possible (in our case, initial) driving force:

$$F_0^{(dr)} = \bar{c}_0 - H\bar{c}_\infty. \quad (45)$$

Here we consider only the external Sherwood number, i.e., the nondimensional rate of transfer of species from the external side of droplet surface into the external flow.

The local and average external Sherwood numbers defined on the basis of the maximum driving force are respectively:

$$Sh_{loc,0} = -2H \cdot D \left. \frac{\partial c^{(1)}}{\partial r} \right|_{r=1} \quad (46)$$

and

$$Sh_0 = -H \cdot D \int_{-1}^1 \left. \frac{\partial c^{(1)}}{\partial r} \right|_{r=1} d\lambda. \quad (47)$$

Corresponding values based on the instantaneous driving force are:

$$Sh_{loc} = \frac{Sh_{loc,0}}{\bar{c}^{(1)}} \quad (48)$$

$$Sh = \frac{Sh_0}{\bar{c}^{(1)}}. \quad (49)$$

The chemical reaction in the external region increases the rate of the extraction, and this increase is characterized by the enhancement factor, which is the ratio of the corresponding mass transfer rates [5]:

$$E = \frac{Sh(Da_{II}^{(2)} \neq 0)}{Sh(Da_{II}^{(2)} = 0)} \quad (50)$$

## COMPUTATIONAL RESULTS AND DISCUSSION

The results of the computations to be presented cover the following ranges of parameters:

$$\begin{aligned} 0.25 &\leq D \leq 4, \\ 0 &\leq Pe^{(2)} \leq 500, \\ 0 &\leq Da_{II}^{(2)} \leq 1000, \\ H &= \mu = 1. \end{aligned}$$

The characteristic time scale was chosen as

$$\tau_* = \tau_{diff}^{(2)}, \quad (51)$$

which is just the Fourier number based on the diffusion coefficient of the external fluid. The times appearing on the plots are expressed in these units. The values of Peclet number  $Pe$  and Damköhler number  $Da$  presented on the plots correspond to  $Pe^{(2)}$  and  $Da_{II}^{(2)}$ , respectively.

To illustrate qualitatively the process of pure mass transfer (no reaction) from the droplet, we present in Figures 1-3 the isocontours of constant species concentration at different times for various levels of external convection ( $Pe^{(2)} = 10, 200, 500$ , respectively). The well known and intuitively expected increase of mass transfer with increasing convection is apparent.

The influence of internal circulation on the development of the mass transfer process is illustrated in Figures 4-5 where we present the isoconcentration contours for the same external Peclet number ( $Pe^{(2)} = 500$ ) and different ratios of internal and external diffusivities ( $D = 0.25$  and  $D = 4.0$ ).

For  $D = 0.25$  the internal convection is much stronger, in the sense that the value of  $Pe^{(1)}$  is larger. As a consequence the concentration isocontours inside the droplet lie close to the internal streamlines, a result already obtained numerically by Johns and Beckmann [7] for the special case of mass transfer resistance solely inside the droplet. The coincidence of internal isocontours with internal streamlines also constituted the basic assumption of Kronig and Brink's model of mass transfer in a circulating drop [6]. From a simple comparison of the isocontour levels in Figures 4 and 5 alone one infers that the mass transfer from a droplet for  $D=4$  is much more intense than for  $D=0.25$ . The reason that the *internal* Peclet number  $Pe^{(1)}$  is greater for  $D = 0.25$  is not that the internal circulation is greater, for it is not ( $\mu = 1$ ), but that the internal diffusivity is smaller. Nonetheless, it is customary for brevity to describe an increase in Peclet number as an increase in convection, rather than the more lengthy but more accurate increase of the ratio of convection to diffusion. In this usage, one may phrase the conclusion drawn from Figures 1-5 as follows: increased convection outside the droplet increases the rate of extraction, but increased convection inside suppresses mass transfer.

The influence of the external reaction rate on the concentration distribution is shown in Figures 2, 6 and 7. As could have easily been anticipated, an increase in  $Da_{II}^{(2)}$  results in faster extraction and an almost immediate disappearance of extracted species outside the droplet (almost no species present for  $Da_{II}^{(2)} = 100$  in Figure 7).

Figures 8 and 9 show the effect of reaction rate on the local Sherwood number. The values of  $Sh_{loc,0}$  go to zero with time for all values of the angle variable  $\vartheta$ , although the surface distribution of Sherwood number based on the instantaneous driving force approaches a nonvanishing asymptote. An increase in the reaction rate thus results in a general increase of mass transfer and of values of the Sherwood numbers, but the temporal variation of values of local Sherwood numbers at different locations is less transparent, warranting further investigation.

Figure 10 reflects the behavior of average Sherwood number  $Sh$  in time for different values of the external Peclet number  $Pe^{(2)}$  for the no-reaction case. The oscillations of  $Sh$  were obtained computationally by different investigators including Johns and Beckmann [7] and Oliver and Chung [9], who solved the conjugate unsteady heat transfer problem, which is mathematically equivalent to the mass transfer problem under consideration when there is no chemical reaction involved. These oscillations are caused by the internal circulation, with the most detailed physical explanation being given by Brignell in [8]. Consequently, the period of these oscillations is smaller and the amplitude greater the higher the Peclet number is. The stronger convection also leads to a higher mass transfer rate as it creates the thinner diffusion boundary layers on the both sides of the droplet surface.

Figure 11 illustrates the influence of the rate of external chemical reaction on the average Sherwood number. The plots confirm the conclusions made above on the increase of the rate of extraction with the increasing external convection and rate of external chemical reaction.

In a more apparent way, this is reflected in Figure 12, where the decrease of the average droplet concentration with time is shown. From this picture we can also deduce the very important conclusion that an increase in the reaction rate beyond some specific value will not benefit the extraction results (the differences between the average droplet concentration for  $Da_{II}^{(2)}$  values of 300 and 1000 are quite small).

Figure 13 shows the effect of reaction rates on the values and temporal evolution of the enhancement factor  $E$ . The oscillations here are the consequences of internal circulation, the same as for the corresponding average Sherwood number on Figure 10. The values of  $E$  corresponding to the same reaction rate are higher for smaller  $Pe^{(2)}$  (lower convection). A possible explanation could be that the corresponding values of  $Da_I^{(2)}$ , which are just the ratios of  $Da_{II}^{(2)}$  and  $Pe^{(2)}$ , are smaller for higher  $Pe^{(2)}$ .

In closing, we want to emphasize that the purpose of this article has been to present the numerical algorithm we have developed and to illustrate some of the kinds of results that can be obtained for this concrete situation. Our subsequent articles will include additional results for other classes of forced convective diffusion-reaction problems for single drops, as well as more detailed analyses of these and other results.

## NOMENCLATURE

- $\bar{c}_0$  -dimensional value of the uniform concentration in the origin of the droplet at  $t = 0$   
 $\bar{c}_\infty$  -dimensional value of the concentration far from the drop  
 $\bar{c}^{(i)}$  -dimensional concentration in the  $i$ -th domain,  $i = 1, 2$   
 $c^{(i)}$  -dimensionless concentration in the  $i$ -th domain,  $i = 1, 2$   
 $D^{(i)}$  -molecular diffusivity of the solute in the fluid in the  $i$ -th domain,  $i = 1, 2$   
 $D$  -molecular diffusivity ratio,  $D^{(1)}/D^{(2)}$   
 $Da_I^{(i)}$  -first Damköhler number in the  $i$ -th domain,  $\frac{k^{(i)} R}{f^{(i)}(\mu) U_\infty}$ ,  $i = 1, 2$   
 $Da_{II}^{(i)}$  -second Damköhler number in the  $i$ -th domain,  $\frac{k^{(i)} R^2}{D^{(i)}}$ ,  $i = 1, 2$   
 $E$  -enhancement factor, eq.(50)  
 $f^{(i)}$  -factor showing the viscosity ratio dependence of the velocity scale in the  $i$ -th domain,  $i = 1, 2$   
 $H$  -distribution coefficient (Henry "law" constant)  
 $k^{(i)}$  -chemical reaction rate constant in the  $i$ -th domain,  $i = 1, 2$   
 $M$  -highest order of the Legendre polynomials used in the expansion in the angular direction  
 $N^{(i)}$  -number of terms in the expansion of radial functions in the  $i$ -th domain,  $i = 1, 2$   
 $Pe^{(i)}$  -Peclet number in the  $i$ -th domain,  $\frac{2 U_\infty f^{(i)}(\mu) R}{D^{(i)}}$ ,  $i = 1, 2$   
 $r$  -dimensionless radial coordinate  
 $R$  -droplet radius  
 $t$  -dimensional time  
 $U_*^{(i)}$  -characteristic velocity scale in the  $i$ -th domain,  $i = 1, 2$   
 $U_\infty$  -velocity of the flow at the infinity  
 $v^{(i)}$  -velocity field in the  $i$ -th domain nondimensionalized by the corresponding velocity scale  $U_*^{(i)}$ ,  $i = 1, 2$   
 $\vartheta$  -polar angle in spherical coordinate system  
 $\lambda = \cos \vartheta$   
 $\mu$  -molecular viscosities ratio,  $\mu^{(1)}/\mu^{(2)}$   
 $\mu^{(i)}$  -molecular viscosity of the fluid in the  $i$ -th domain,  $i = 1, 2$   
 $\tau$  -dimensionless time  
 $\tau_{conv}^{(i)}$  -convection time scale in the  $i$ -th domain,  $\frac{R}{f^{(i)}(\mu) U_\infty}$ ,  $i = 1, 2$   
 $\tau_{diff}^{(i)}$  -diffusion time scale in the  $i$ -th domain,  $\frac{R^2}{D^{(i)}}$ ,  $i = 1, 2$   
 $\tau_{rxn}^{(i)}$  -chemical reaction time scale in the  $i$ -th domain,  $\frac{1}{k^{(i)}}$ ,  $i = 1, 2$

## REFERENCES

- [1] J. P. Boyd, *Chebyshev and Fourier Spectral Methods*. Springer-Verlag (1989).
- [2] C. Canuto, M. Y. Hussaini, A. Quarteroni, *Spectral Methods in Fluid Dynamics*. Springer-Verlag (1988).
- [3] G. H. Golub and C. F. Van Loan, *Matrix Computations*. Johns Hopkins University Press (1989).
- [4] C. A. J. Fletcher, *Computational Techniques for Fluid Dynamics*. Springer-Verlag (1988).
- [5] R.B. Bird, W. E. Stewart, E. N. Lightfoot, *Transport Phenomena*. John Wiley & Sons (1966).
- [6] R. R. Kronig and J. C. Brink, On the theory of extraction from falling droplets. *Appl. Sci. Res. A2*, 142-155 (1950)
- [7] L. E. Johns, Jr and R. B Beckmann, Mechanism of dispersed-phase mass transfer in viscous, single-drop extraction systems. *A.I.Ch.E. Jl* 12, 10-16 (1966).
- [8] A. S. Brignell, Solute extraction from an internally circulating spherical liquid drop. *Int. J. Heat Mass Transfer* 18, 61-68 (1975).
- [9] D. L. R. Oliver, J. N. Chung, Conjugate unsteady heat transfer from a spherical droplet at low Reynolds numbers. *Int. J. Heat Mass Transfer* 29, 879-887 (1986).
- [10] P. R. Spalart, A spectral method for external viscous flows. *Contemporary mathematics* 28, 315-335 (1984).
- [11] C. E. Grosch, S. A. Orszag, Numerical solution of problems in unbounded regions: coordinate transforms. *J. of Comput. Phys.* 25, 273-296 (1977).
- [12] B. Fornberg, A numerical study of steady viscous flow past a circular cylinder, *J. Fluid Mech.*, 98, 819-855, 1980
- [13] A. T. Patera, A spectral element method for fluid dynamics: laminar flow in a channel expansion. *J. of Comput. Phys.* 54, 468-488 (1984).
- [14] D. Gottlieb, S. A. Orszag, *Numerical Analysis of Spectral Methods*. SIAM (1977)
- [15] A. E. Hamielec, A. I. Johnson, Viscous flow around fluid spheres at intermediate Reynolds numbers. *Can. J. Chem. Engng.* 40, 2, 41 (1962).
- [16] F. Cooper, Heat transfer from a sphere to an infinite medium. *Int. J. Heat Mass Transfer* 20, 991-993 (1977).

Table 1: Coefficients in eq.(1) depending on the choice of  $\tau_*$  ( $i, j = 1, 2$ )

$\tau_*$	$K_c^{(i)}$	$K_d^{(i)}$	$K_r^{(i)}$
$\tau_{\text{diff}}^{(j)}$	$\frac{Pe^{(i)}}{2} \cdot \frac{D^{(i)}}{D^{(j)}}$	$\frac{D^{(i)}}{D^{(j)}}$	$Da_{II}^{(i)} \cdot \frac{D^{(i)}}{D^{(j)}}$
$\tau_{\text{conv}}^{(j)}$	$\frac{f^{(i)}(\mu)}{f^{(j)}(\mu)}$	$\frac{2}{Pe^{(i)}} \cdot \frac{f^{(i)}(\mu)}{f^{(j)}(\mu)}$	$Da_I^{(i)} \cdot \frac{f^{(i)}(\mu)}{f^{(j)}(\mu)}$
$\tau_{\text{rxn}}^{(j)}$	$\frac{1}{Da_I^{(i)}} \cdot \frac{k^{(i)}}{k^{(j)}}$	$\frac{1}{Da_{II}^{(i)}} \cdot \frac{k^{(i)}}{k^{(j)}}$	$\frac{k^{(i)}}{k^{(j)}}$

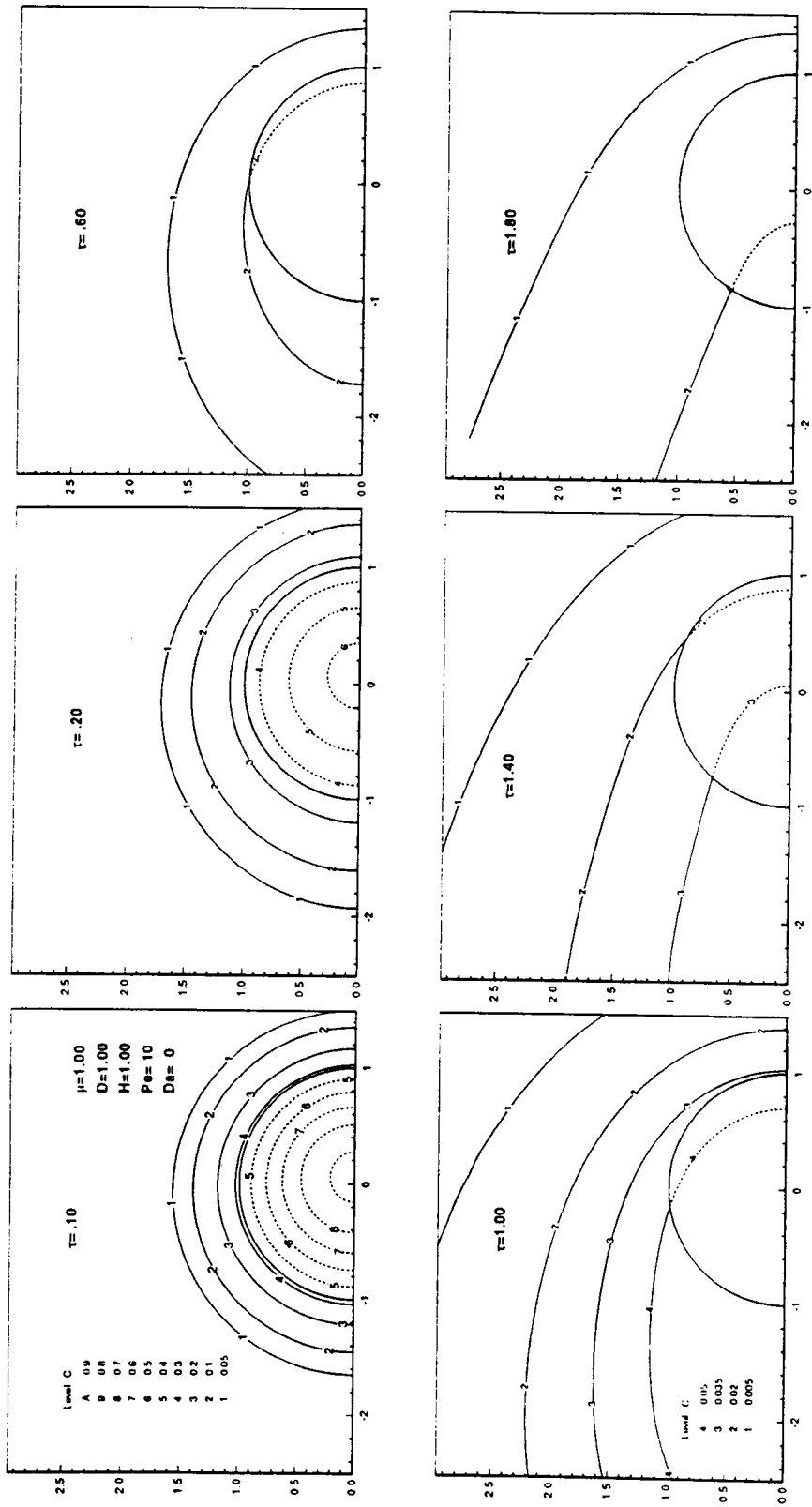


Fig. 1 Isoconcentration curves at different time moments for  $Pe=10$

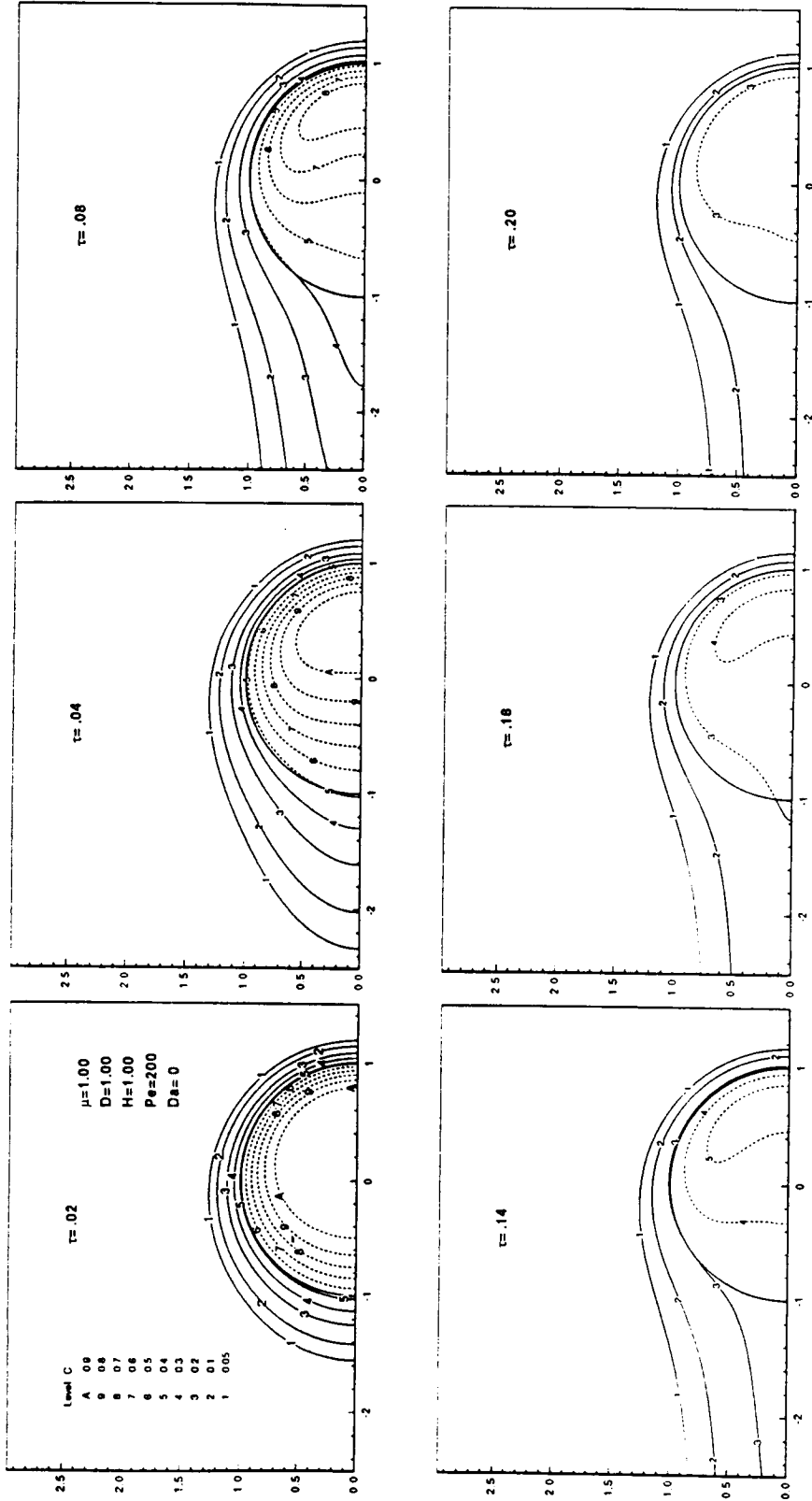


Fig. 2 Isoconcentration curves at different time moments for  $Pe=200$

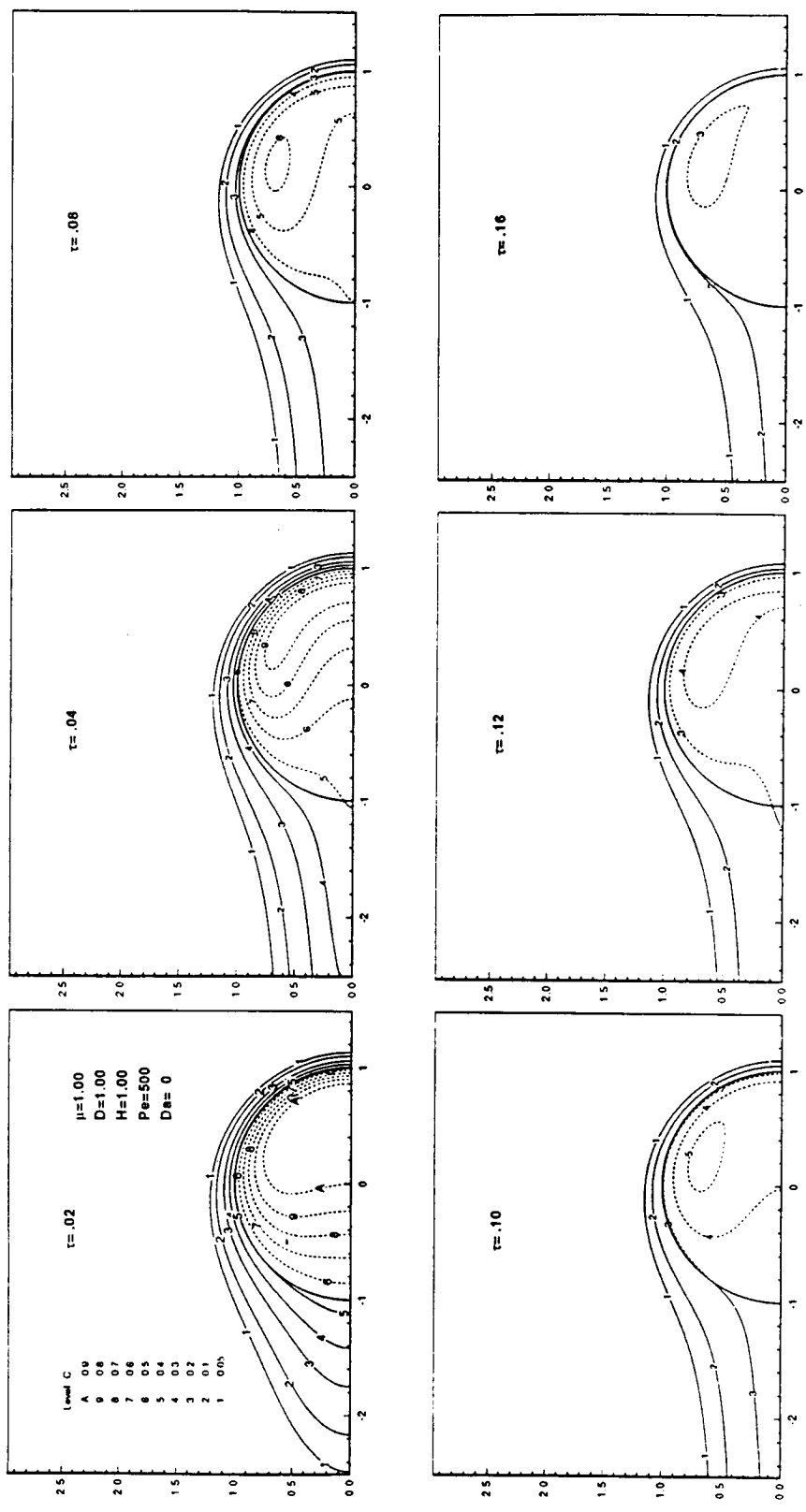


Fig. 3 Isoconcentration curves at different time moments for  $Pe=500$

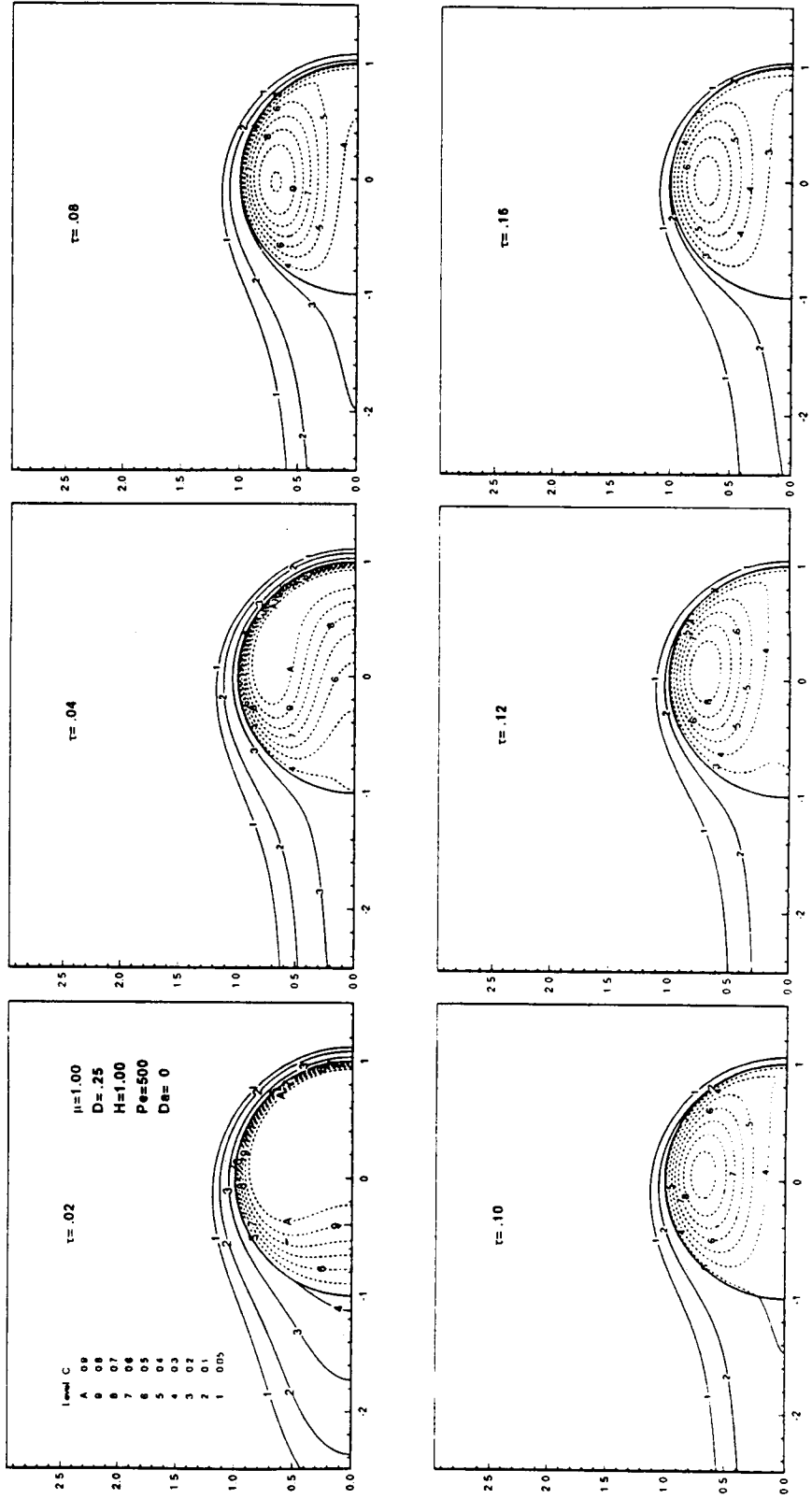


Fig. 4 Isoconcentration curves at different time moments for  $Pe=500$  and  $D=.25$

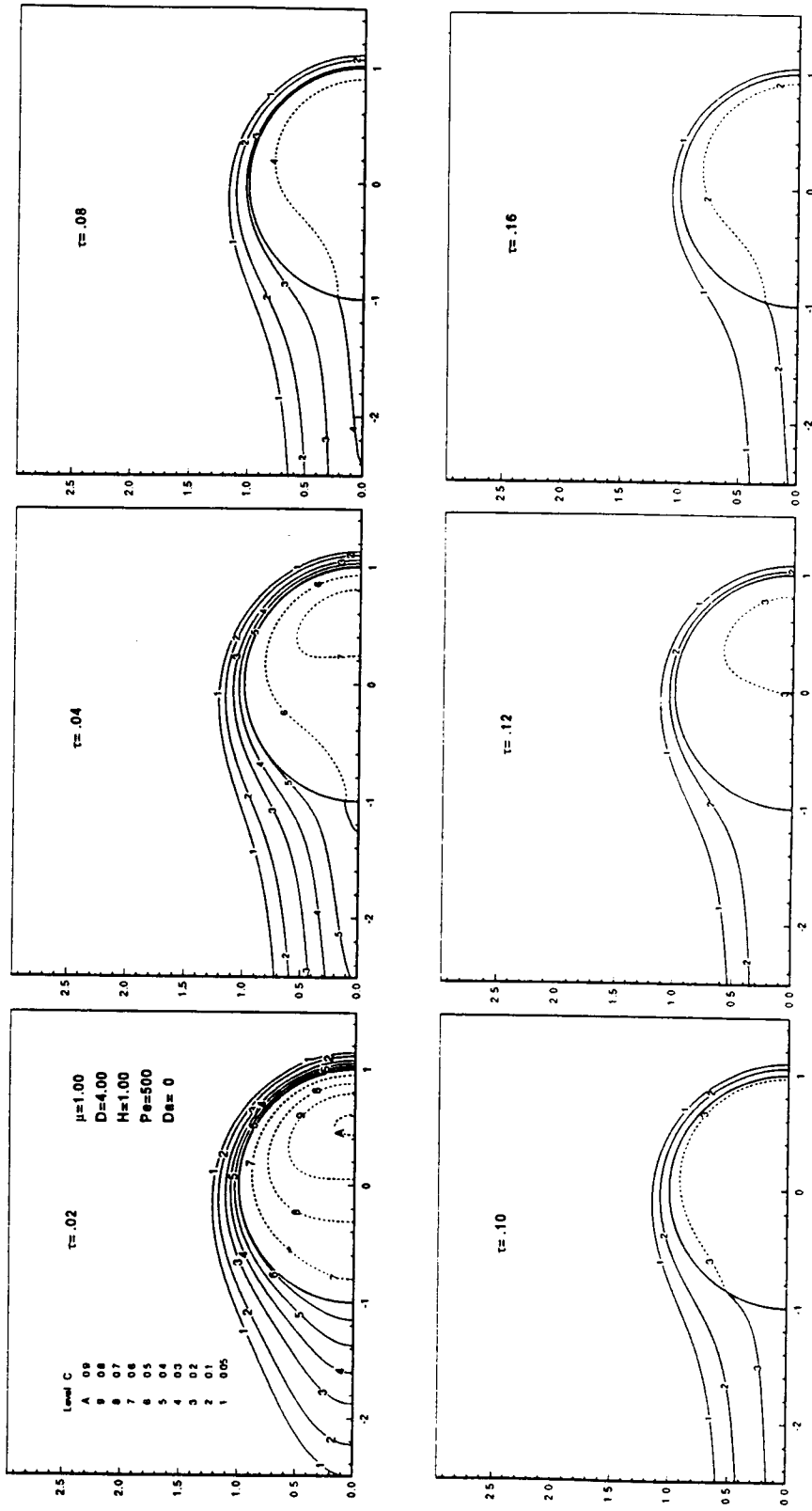


Fig. 5 Isoconcentration curves at different time moments for  $Pe=500$  and  $D=4.0$

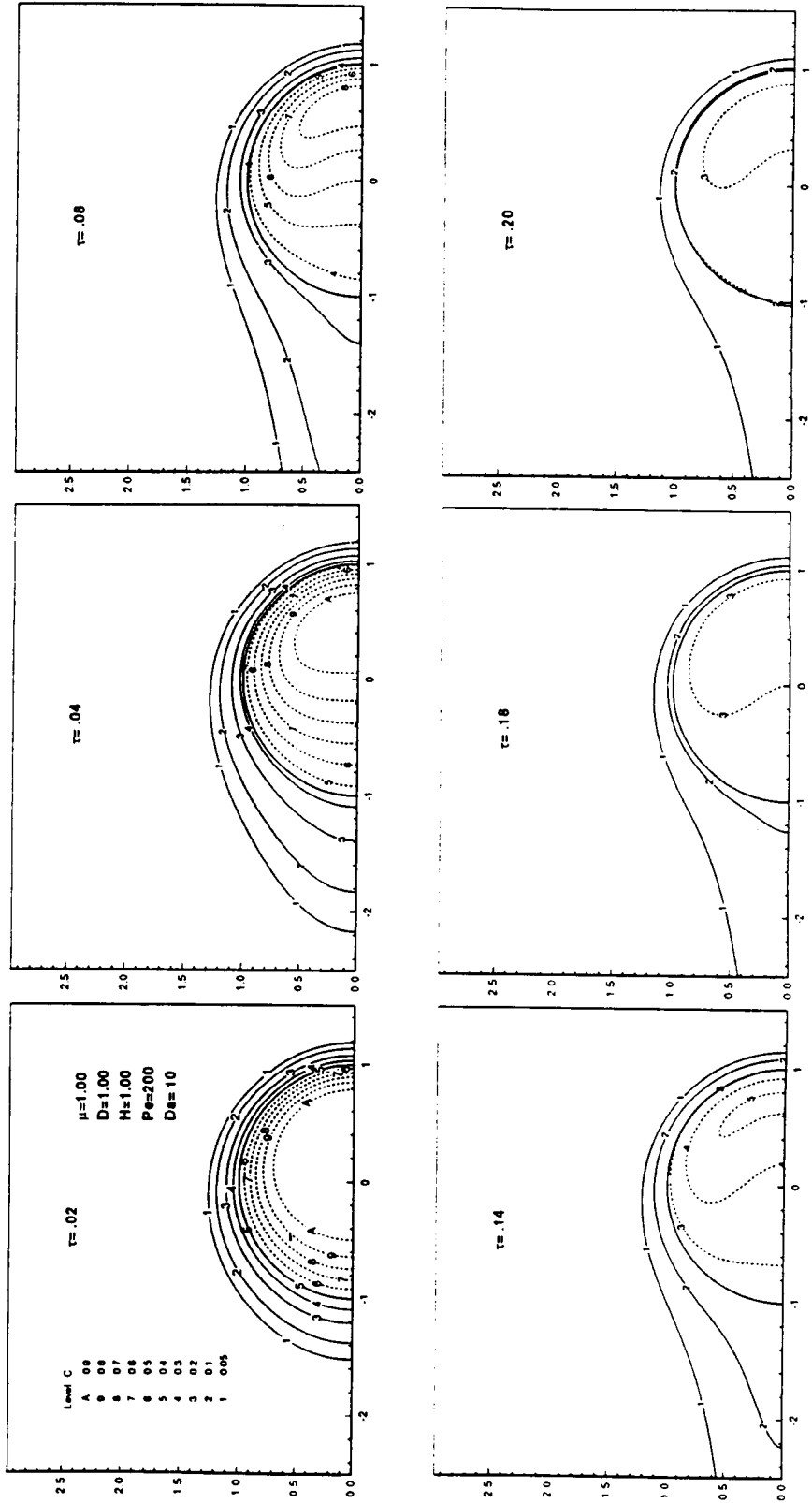


Fig. 6 Isoconcentration curves at different time moments for  $Pe=200$  and  $Da=10$

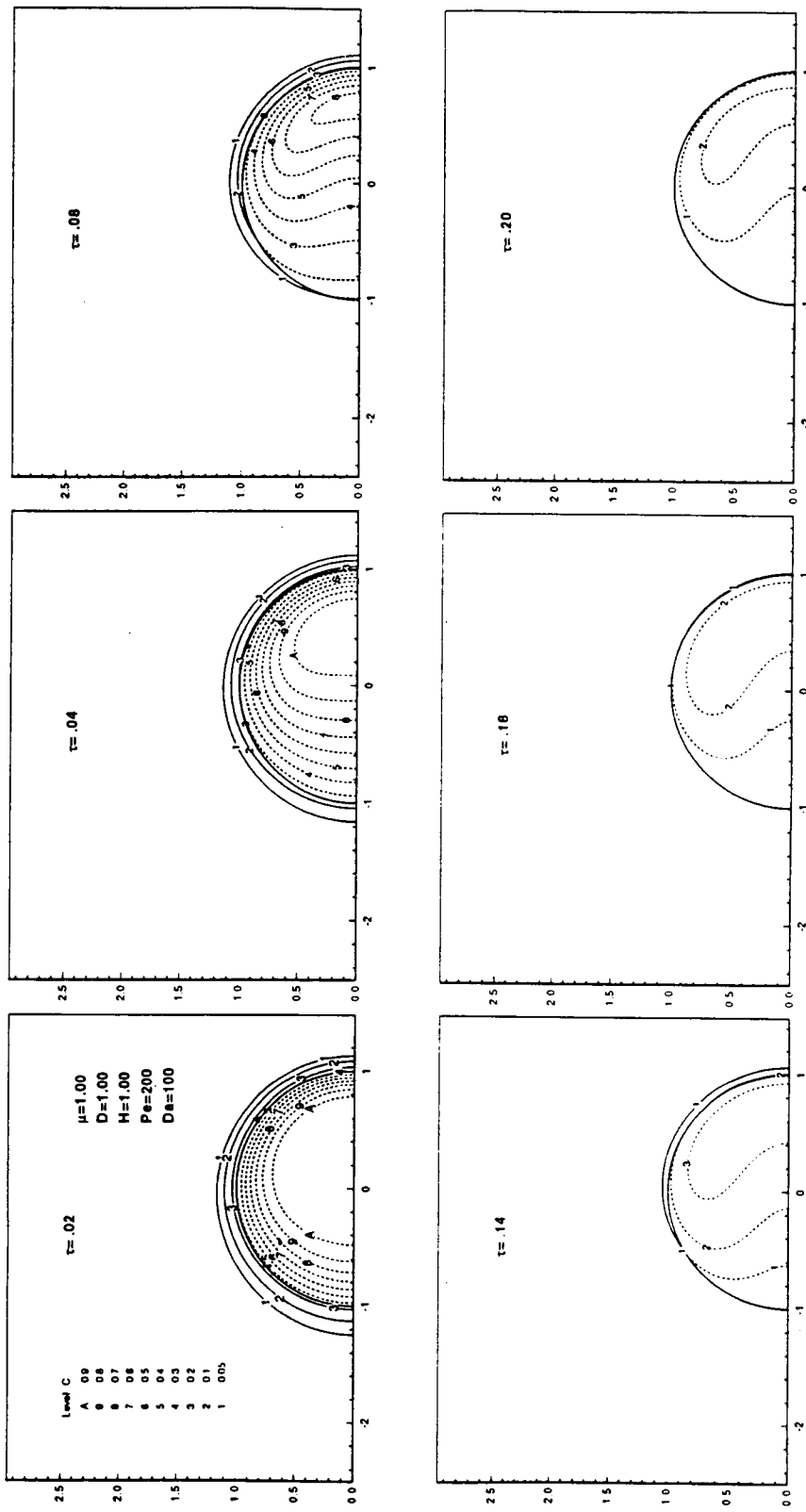


Fig. 7 Isoconcentration curves at different time moments for  $Pe=200$  and  $Da=100$

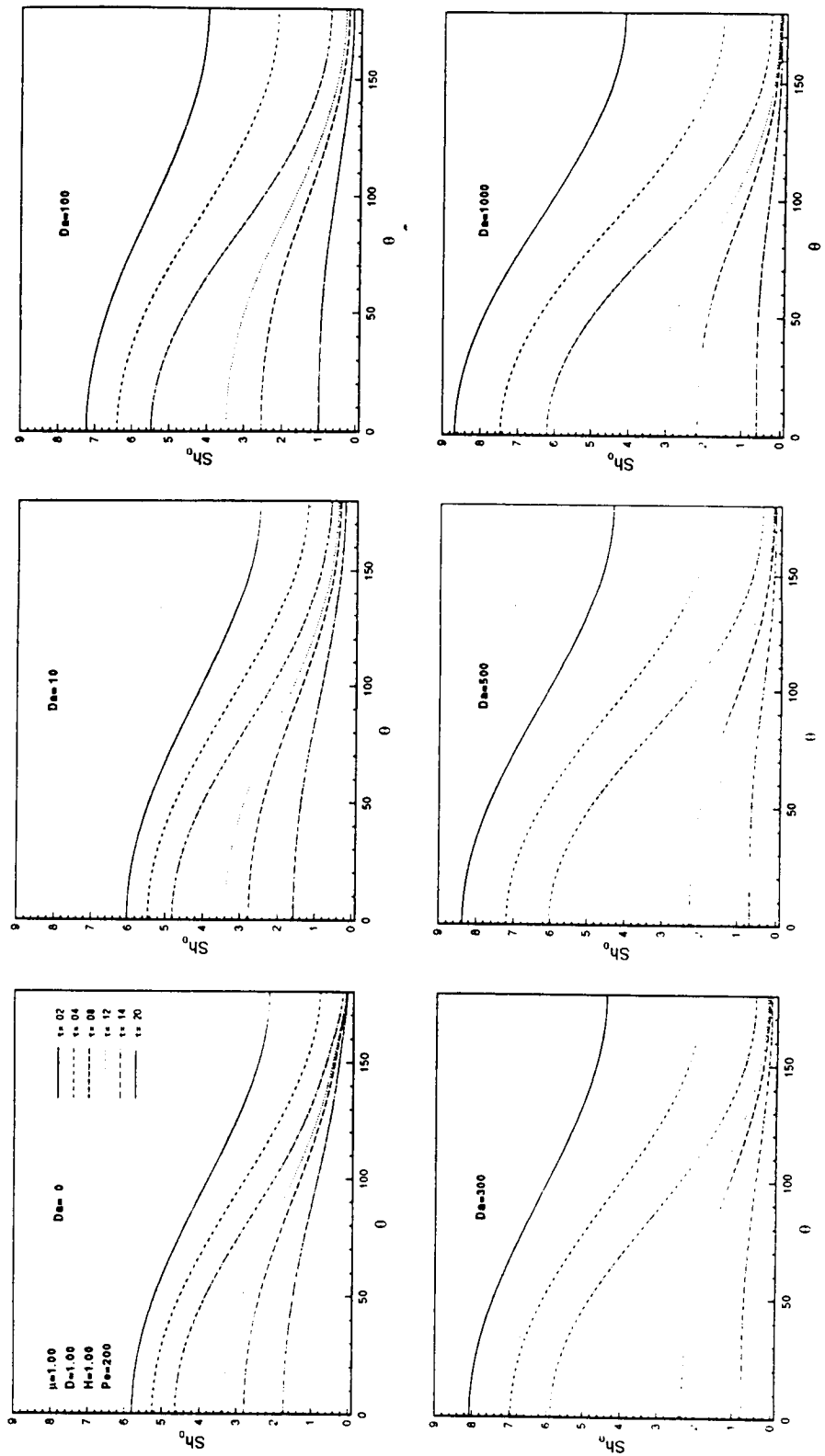


Fig. 8 Distribution of the values of local Sherwood number  $Sh_0$  at  $Pe=200$  for different values of  $Da$

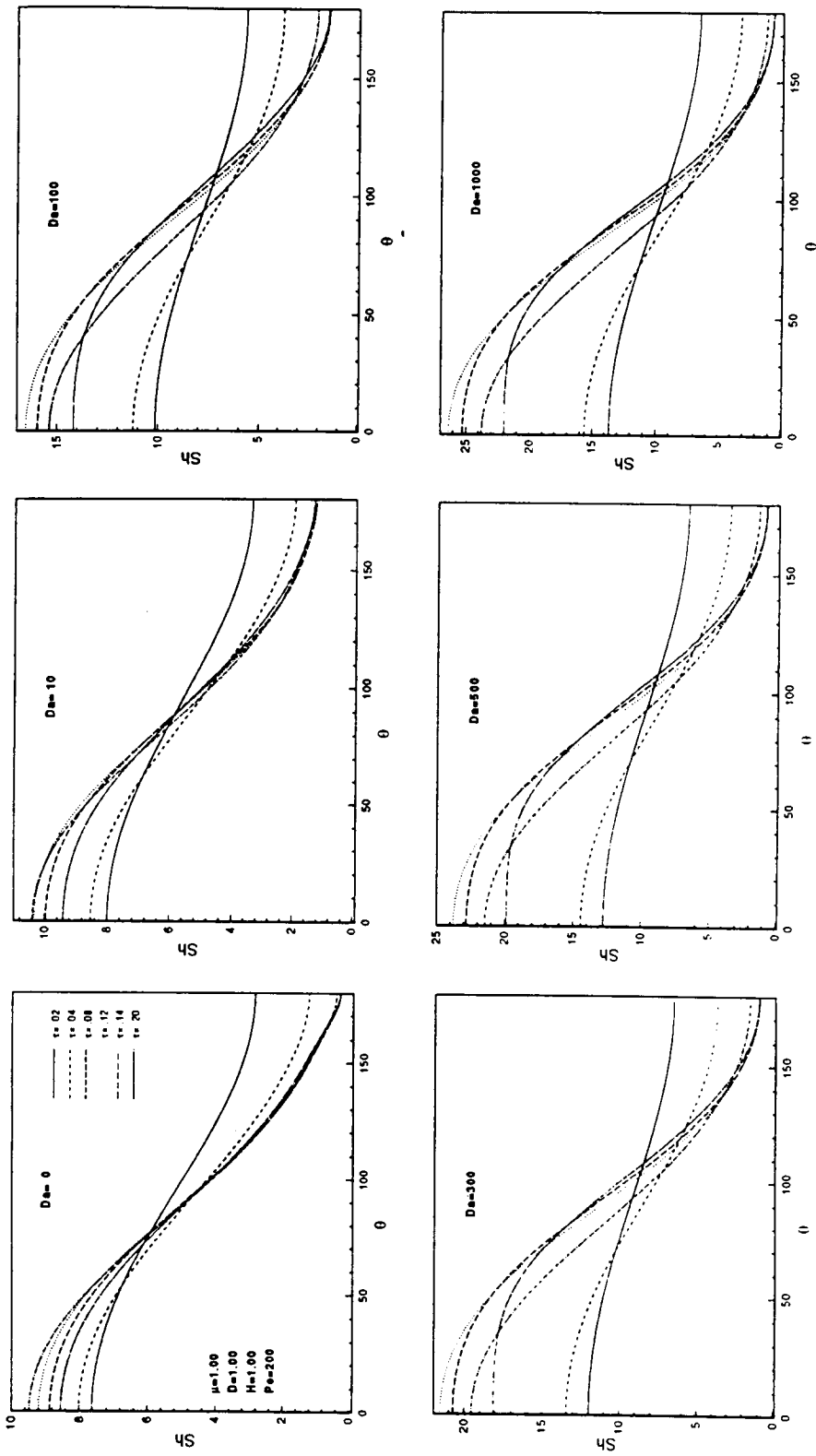


Fig. 9 Distribution of the values of local Sherwood number  $Sh$  at  $Pe=200$  for different values of  $Da$

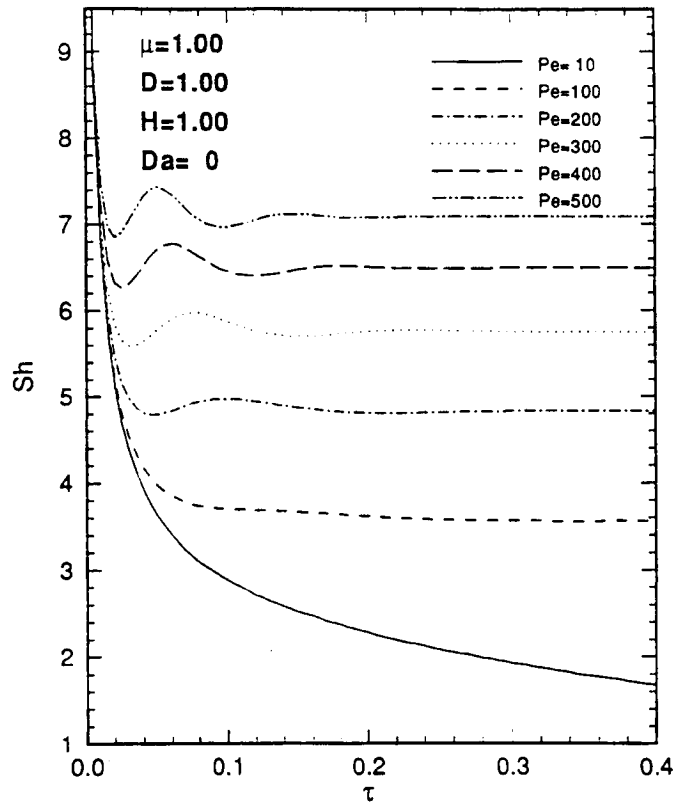


Fig. 10 Time evolution of average Sherwood number  $Sh$  for  $Da=0$  at different values of  $Pe$

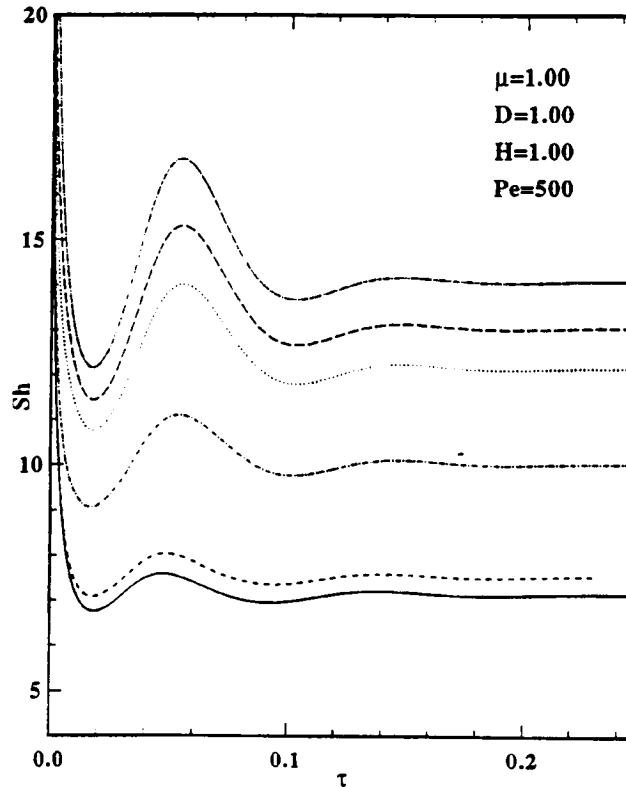
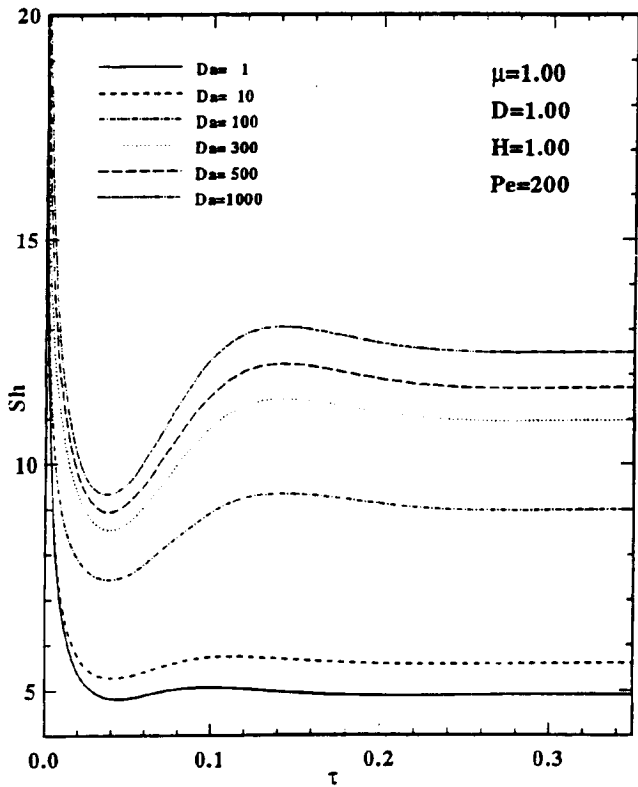


Fig. 11 Effect of reaction rate on average Sherwood number  $Sh$  for  $Pe=200$  and  $Pe=500$

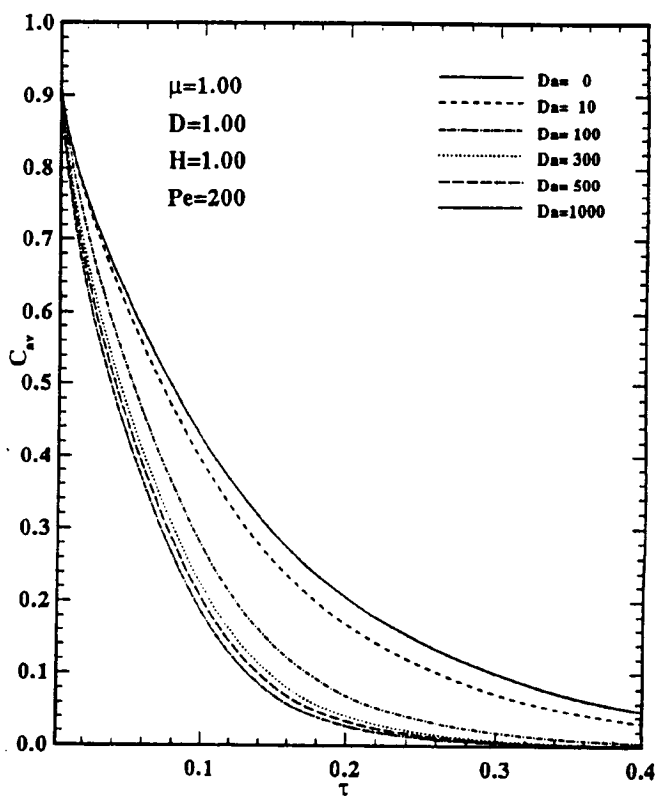
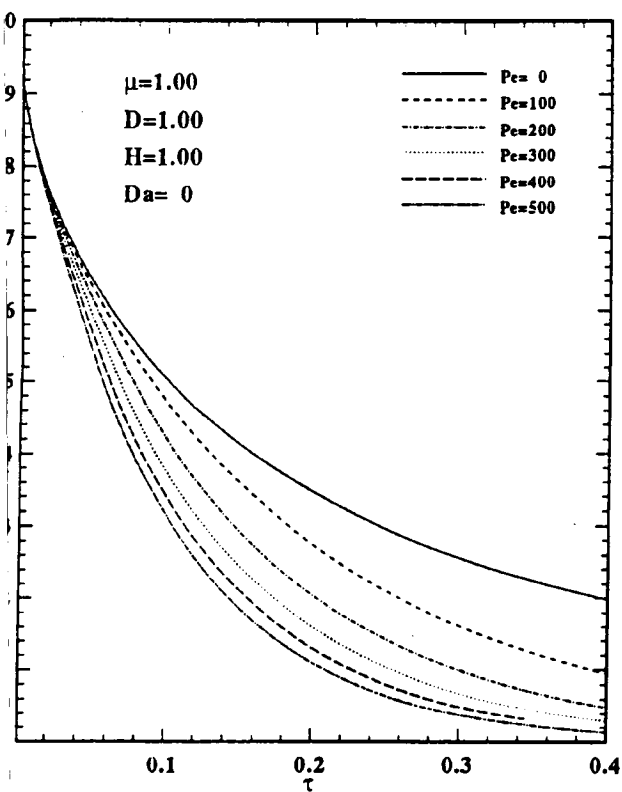


Fig. 12 Time evolution of average droplet concentration